

Estimates for Lorentz factors of gamma-ray bursts from early optical afterglow observations

Romain Hascoët¹, Andrei M. Beloborodov

*Physics Department and Columbia Astrophysics Laboratory, Columbia University, 538 West
120th Street New York, NY 10027*

Frédéric Daigne, Robert Mochkovitch

*Institut d'Astrophysique de Paris, UMR 7095 Université Pierre et Marie Curie - CNRS, 98 bis
boulevard Arago, Paris 75014, France*

ABSTRACT

The peak time of optical afterglow may be used as a proxy to constrain the Lorentz factor Γ of the gamma-ray burst (GRB) ejecta. We revisit this method by including bursts with optical observations that started when the afterglow flux was already decaying; these bursts can provide useful lower limits on Γ . Combining all analyzed bursts in our sample, we find that the previously reported correlation between Γ and the burst luminosity L_γ does not hold. However, the data clearly shows a lower bound Γ_{\min} which increases with L_γ . We suggest an explanation for this feature: explosions with large jet luminosities and $\Gamma < \Gamma_{\min}$ suffer strong adiabatic cooling before their radiation is released at the photosphere; they produce weak bursts, barely detectable with present instruments. To test this explanation we examine the effect of adiabatic cooling on the GRB location in the $L_\gamma - \Gamma$ plane using a Monte Carlo simulation of the GRB population. Our results predict detectable on-axis “orphan” afterglows. We also derive upper limits on the density of the ambient medium that decelerates the explosion ejecta. We find that the density in many cases is smaller than expected for stellar winds from normal Wolf-Rayet progenitors. The burst progenitors may be peculiar massive stars with weaker winds or there might exist a mechanism that reduces the stellar wind a few years before the explosion.

Subject headings: gamma-rays: bursts

1. Introduction

The prompt emission of gamma-ray bursts (GRBs) is likely produced by dissipative mechanisms inside the relativistic ejecta of the explosion, while the GRB afterglow is associated with the

¹hascoet@astro.columbia.edu

ejecta deceleration by a circum-burst medium (see e.g. Piran 2004 for a review). The afterglow emission is attributed to a relativistic blast wave that involves a pair of shocks – forward and reverse.

One of the most important parameters of GRBs is the Lorentz factor of the relativistic ejecta, Γ , as the models of the prompt and afterglow emissions strongly depend on its value. Useful constraints on Γ may be derived using the timescale and spectrum of the prompt GRB (Paczynski 1986; Goodman 1986), which typically gives $\Gamma > 100$ (e.g. Lithwick & Sari 2001; Hascoët et al. 2012). Another possible way to constrain the GRB Lorentz factor is to use the afterglow peak time T_p as a proxy for the deceleration time of the blast wave, T_{dec} , at which the dissipation rate peaks (e.g. Meszaros & Rees 1997; Sari & Piran 1999). Using this method Liang et al. (2010, 2013) and Ghirlanda et al. (2012) studied a sample of GRBs with detected optical peaks and found a correlation between Γ and the burst luminosity L_γ .

The key assumption of this method, $T_p \sim T_{\text{dec}}$, is questionable, as optical emission could reach its peak at a different time. This possibility is illustrated by the simple model of synchrotron emission from a self-similar blast-wave, where the optical light curve can peak at $T_p \gg T_{\text{dec}}$ (e.g. Sari et al. 1998). However, observations conflict with the late- T_p models and lend some support to the $T_p \sim T_{\text{dec}}$ assumption. In many bursts, optical emission peaks early and steeply, as may be expected at T_{dec} .¹ The optical peak may be dominated by the forward- or reverse-shock emission (e.g. Meszaros & Rees 1997; Sari & Piran 1999; Uhm & Beloborodov 2007; Genet et al. 2007). In this paper, we accept $T_p \simeq T_{\text{dec}}$ as a reasonable assumption and investigate its implications.

In Sections 2 and 3, we extend the previous analysis by including bursts whose afterglow peaked before observations started, which provides a useful upper limit on T_p . We also identify the cases where the blast wave at T_p is significantly slower than the ejecta, which corresponds to a relativistic reverse shock; in these cases the measurement of T_p provides only a lower bound on the ejecta Lorentz factor Γ . Our analysis does not support the existence of the $L_\gamma - \Gamma$ correlation claimed in previous studies. Instead, the data shows a lack of bright bursts with low Lorentz factors. In Section 4, we suggest an explanation of this fact. Section 5 summarizes our results and discusses implications of observed T_p for the nature of the circum-burst medium.

¹This expectation depends on the model for the circum-burst density. A steep rise is firmly predicted if the density is uniform, $\rho = \text{const}$, but questionable if $\rho \propto R^{-2}$ (wind-type medium, Chevalier & Li 2000). In the latter case, additional effects such as e^\pm pair loading could produce the steep rise toward the peak (Beloborodov 2002).

2. Sample

2.1. Bursts with detected optical afterglow peaks

Table 1 gives the list of 20 GRBs with *detected* early afterglow peaks that are included in our sample. This list is a selection from the GRB samples of Liang et al. (2010); Lü et al. (2012); Liang et al. (2013), where we keep only bursts with reliable detection of the peak time. We removed (1) GRBs that have optical light-curves with more than one bump, making the peak measurement ambiguous, (2) GRBs for which the peak was measured during a plateau phase (i.e. where the optical light-curve is flat in logarithmic scale), and (3) GRBs with optical light-curves that are sampled too sparsely or whose temporal range is too small to provide significant constraints on T_p .

The redshift-corrected peak times $T_p = T_p^{\text{obs}}/(1+z)$ are shown in Figure 1 versus the GRB isotropic equivalent gamma-ray energy E_γ and the corresponding average luminosity

$$L_\gamma = \frac{E_\gamma}{T_\gamma}, \quad (1)$$

where

$$T_\gamma = \frac{T_{90}}{1+z}, \quad (2)$$

and T_{90} is an approximate measure of the observed burst duration (time during which 90% of the emission is received). One can notice a good correlation between T_p and L_γ (or E_γ); we argue below that this correlation is spurious.

2.2. Bursts with upper limits on T_p

For some bursts the peak is not observed because observations start too late. These bursts are also useful for our purposes, as some of them give strong upper-limits on T_p . A sample of such GRBs is listed in Table 2 and the corresponding upper limits are shown in Figure 1. The number of available strong limits (24) is comparable to the number of peak detections. The limits are robust. For many bursts in the sample, the optical decay was already well established when the observations started, without any evidence for an increasing decay index. This suggests that the peak was reached well before the beginning of observations.

The obtained limits on T_p are never below a few tens of seconds, which reflects the typical delay in response of robotic optical telescopes to alerts from γ -ray telescopes.² Note also that the limits tend to be less constraining for weak (low E_γ) bursts. It is easier to obtain strong limits for bright

²Due to a fortunate chain of events, optical observations of GRB 080319B started *before* the γ -ray trigger (Racusin et al. 2008). However in this special case the rise of the optical afterglow is hidden by the bright prompt optical component.

Table 1: Bursts with detected optical peaks.

| GRB | z | $E_{\gamma,52}$ | T_p^{obs} | T_{90} | References |
|---------|---------|-----------------|--------------------|-----------|------------|
| 990123 | 1.60 | 436.52±60.31 | 47±10 | 63.3±0.3 | 1, 2 |
| 050820A | 2.612 | 159.2±12.4 | 477±6 | 600±50 | 2, 3 |
| 060418 | 1.489 | 48.6±10.6 | 170±5 | 52±1 | 2, 3, 4 |
| 060605 | 3.78 | 2.8±0.5 | 590±45 | 19±1 | 2, 3 |
| 060607A | 3.082 | 23.4±1.5 | 179±3 | 100±5 | 2, 3, 4 |
| 061007 | 1.261 | 421±41.9 | 77±1 | 75±5 | 2, 3 |
| 070318 | 0.836 | 1.3±0.3 | 507±46 | 63±5 | 2, 3 |
| 070419A | 0.97 | 0.2±0.02 | 765±30 | 112±2 | 2, 3 |
| 071010B | 0.947 | 1.7±0.9 | 287±145 | 35.74±0.5 | 2, 3 |
| 071031 | 2.692 | 3.9±0.6 | 1213±2 | 180±10 | 5, 3 |
| 080603A | 1.68742 | 2.2±0.8 | 1600±400 | 150±10 | 6, 7 |
| 080710 | 0.845 | 0.8±0.4 | 1934±46 | 120±17 | 2, 3 |
| 080810 | 3.35 | 30±20 | 117±2 | 108±5 | 2, 3 |
| 081008 | 1.967 | 2.8±0.5 | 163±2 | 185±39 | 8, 3 |
| 081203A | 2.1 | 17±4 | 295±2 | 294±71 | 9, 3 |
| 090313 | 3.375 | 4.6±0.5 | 1315±109 | 78±19 | 2, 3 |
| 090812 | 2.452 | 45.9±6 | 71±8 | 70±5 | 10, 3 |
| 091029 | 2.752 | 7.4±0.74 | 328±50 | 39.2±5 | 11, 2 |
| 100906A | 1.727 | 33.4±3 | 101±4 | 114.4±1.6 | 2, 3 |
| 110205A | 2.22 | 56±6 | 948±3 | 257±25 | 2, 3 |

References: (1) Liang et al. 2010; (2) Lü et al. 2012; (3) Liang et al. 2013; (4) Molinari et al. 2007; (5) Stamatikos et al. 2007; (6) Martin-Carrillo et al. 2008; (7) Guidorzi et al. 2011; (8) Yuan et al. 2010; (9) Ukwatta et al. 2008; (10) Stamatikos et al. 2009; (11) Grupe et al. 2009

bursts for a few reasons: they are easily localized by γ -ray telescopes; they have brighter afterglows (Gehrels et al. 2008); and they have higher redshifts which move T_p to a later $T_p^{\text{obs}} = (1+z)T_p$

While it is easy to miss an early optical peak, $T_p < 100$ s, we are not aware of any selection effects that could lead to preferential non-detection of late peaks $T_p \sim 10^2 - 10^3$ s. In this range, the data should represent the true distribution of T_p . The data presented in Figure 1 may be summarized as follows: *there is no intrinsic correlation between T_p and L_γ (or E_γ). Instead we observe a lack of bright bursts with late afterglow peaks.* For a given L_γ , there appears to exist a maximum peak time $T_{p,\text{max}}(L_\gamma)$ which corresponds to the blue boundary in Figure 1. A crude approximation to this boundary is given by $T_{p,\text{max}}(L_\gamma) \sim 200 L_{\gamma,52}^{-3/5}$ s.

3. Estimates for Γ

The GRB afterglow is likely emitted by the blast wave resulting from the interaction of the relativistic ejecta with the ambient medium. The blast wave involves two shocks: the forward shock sweeping the external medium and the reverse shock propagating back into the relativistic ejecta. As discussed in Section 1, it is reasonable to assume that the afterglow peaks at the deceleration time T_{dec} when most of the ejecta energy has been transmitted to the blast-wave through the reverse shock. This happens at the “deceleration radius,”

$$R_{\text{dec}} = \left(\frac{3-s}{4\pi c^2} \frac{E_{\text{ej}}}{\Gamma_{\text{bw}}^2 \rho_{\text{dec}}} \right)^{\frac{1}{3}}, \quad (3)$$

where E_{ej} is the energy of the ejecta and Γ_{bw} is the Lorentz factor of the blast wave at R_{dec} ; ρ_{dec} is the external density at R_{dec} , and s describes the slope of the external density profile, $s = d \ln \rho / d \ln R$. A uniform medium is described by $s = 0$ and a wind medium by $s = 2$. We assume that the afterglow peaks at the deceleration time,

$$T_p \simeq T_{\text{dec}} \simeq \frac{R_{\text{dec}}}{2\Gamma_{\text{bw}}^2 c}. \quad (4)$$

Then the measured T_p provides an estimate for the blast wave Lorentz factor,

$$\Gamma_{\text{bw}} = \left[\frac{3-s}{32\pi c^5} \frac{1-\eta}{\eta} \frac{E_\gamma}{\rho_{\text{dec}} T_p^3} \right]^{\frac{1}{8}}, \quad (5)$$

where η is the fraction of the initial energy of the GRB ejecta that is converted into prompt radiation.

Two aspects of Equation (5) should be noted: (1) the estimate depends on the poorly known ambient density as $[\rho_{\text{dec}}/(3-s)]^{-1/8}$ and the prompt efficiency as $[\eta/(\eta-1)]^{-1/8}$. (2) The estimate gives the Lorentz factor of the *blast wave*, Γ_{bw} , not the ejecta Lorentz factor Γ .

We expect $\Gamma \simeq \Gamma_{\text{bw}}$ if $T_p \gg T_\gamma$. Indeed, T_p is associated with the time it takes the ejecta to transfer most of its energy to the blast wave, i.e. the time it takes the reverse shock to cross

the main, most energetic part of the ejecta of thickness $\Delta \simeq cT_\gamma$. The crossing time Δ/v_{rs} is long and gives $T_p \sim (c/v_{\text{rs}})T_\gamma \gg T_\gamma$ if the reverse shock is non relativistic, $v_{\text{rs}} \ll c$, which is equivalent to $\Gamma \simeq \Gamma_{\text{bw}}$. In this case Equation (5) effectively gives an estimate of the mean Lorentz factor Γ of the ejecta. In contrast if $T_p \lesssim T_\gamma$, the reverse shock may be highly relativistic. Then Γ_{bw} is significantly smaller than Γ and Equation (5) significantly underestimates Γ . GRBs with $T_p \lesssim T_\gamma$ are highlighted in red in Figure 1.

Note that T_γ that we use as a measure of the GRB duration may overestimate the duration of the main part of the GRB if the burst has a temporally extended tail of relatively weak emission. For such bursts $T_{\text{dec}} < T_\gamma$ is possible. A better estimate for T_γ would give $T_{\text{dec}} \simeq T_\gamma$, so that T_p is not smaller than T_γ . In agreement with theoretical expectations, we found no burst in our sample where the optical afterglow peaks before the main part of the GRB emission has been received.

Equation (5) assumes a static external medium and neglects the fact that the prompt GRB radiation exerts pressure and accelerates the medium ahead of the blast wave (Thompson & Madau 2000; Beloborodov 2002). This pre-acceleration is strong (relativistic) up to the radius,

$$R_{\text{acc}} = 2 \times 10^{15} (E_{\gamma,52})^{1/2} \text{ cm}. \quad (6)$$

If R_{acc} exceeds R_{dec} given by Equation (5), the true deceleration radius is increased, and the dissipation rate peaks at

$$T_p = \frac{R_{\text{acc}}}{2\Gamma_{\text{bw}}^2 c} \simeq 4(E_{\gamma,52})^{1/2} \left(\frac{\Gamma_{\text{bw}}}{100} \right)^{-2} \text{ s}. \quad (7)$$

We found $R_{\text{acc}} < R_{\text{dec}}$ for all bursts in our GRB sample as long as $\rho_{\text{dec}}/m_p \lesssim 10^3 \text{ cm}^{-3}$. For most bursts in our sample, $\rho_{\text{dec}}/m_p \gtrsim 10^3 \text{ cm}^{-3}$ would imply low values for Γ , which would contradict the constraint from the prompt emission (see discussion in Section 5.2). Therefore we will assume $\rho_{\text{dec}}/m_p \lesssim 10^3 \text{ cm}^{-3}$ and neglect the pre-acceleration effect.

Using Equation (5) we estimated Γ for each burst in the sample (Figure 2). We fixed $\eta = 0.5$ and $s = 2$ in our numerical estimates; the uncertainty in their exact values weakly affects the results. If only the peak “detections” are considered, Figure 2 would suggest that there is a correlation between Γ and L_γ . However, the numerous lower limits show that the upper part of the diagram must be broadly populated by GRBs. Also note that four detections of T_p correspond to the relativistic reverse shock regime and give only lower limits on Γ . We conclude that there is no evidence for a correlation between L_γ and Γ . However the lack of bright bursts with low Γ appears to be a robust feature.

Figure 3 illustrates how the GRB sample is transformed from $L_\gamma - T_p$ plane to $L_\gamma - \Gamma_{\text{bw}}$ plane, following the relation between Γ_{bw} and T_p , $\Gamma_{\text{bw}} \propto E_\gamma^{1/8} T_p^{-3/8}$ (Equation (5)). This transformation compresses the sample along the Γ_{bw} axis and induces a dependence of Γ_{bw} on L_γ with a positive slope of 1/8. In combination with the selection effect that suppresses short- T_p and low- L_γ bursts in the sample, this enhances the spurious correlation between L_γ and Γ .

As mentioned in Section 1, the key assumption that the optical afterglow peaks at the decel-

eration radius may not be reliable. Therefore, it is useful to consider a more general model where the afterglow peaks at a radius R_p related to Γ and L_γ by

$$R_p \propto \Gamma^\alpha L_\gamma^\beta. \quad (8)$$

The simplest model with $\rho_{\text{dec}} = \text{const}$ corresponds to $\alpha = -2/3$ and $\beta = 1/3$ (see Equation (3)). For other values of α, β , the observed upper boundary $T_p^{\text{max}} \propto L_\gamma^\lambda$ (where $\lambda \sim -3/5$; see Figure 1) in the $L_\gamma - T_p$ diagram still transforms into a lower-boundary $\Gamma_{\text{min}} \propto L_\gamma^{(\lambda-\beta)/(\alpha-2)}$ in the $L_\gamma - \Gamma$ diagram. As an illustration, Figure 4 shows Γ estimated assuming $\alpha = \beta = 0$ (i.e. $R_p = \text{const}$). The results are similar to those in Figure 2. The conclusion that Γ_{min} grows with L_γ holds as long as $(\lambda - \beta)/(\alpha - 2) > 0$. Violation of this condition would require α and β that are significantly different from $\alpha = -2/3$ and $\beta = 1/3$. If $\alpha \simeq 2$ then T_p weakly depends on Γ , and cannot be used to estimate Γ .

4. Lack of bright bursts with a large T_p : a result of adiabatic cooling?

4.1. Adiabatic cooling below the photosphere

The photospheric radius R_* (the characteristic radius where the explosion ejecta becomes transparent to Thomson scattering) is given by

$$R_* \approx 3 \times 10^{12} \kappa_{0.2} L_{52} \Gamma_2^{-3} \text{ cm}, \quad (9)$$

where L is the isotropic power of the outflow, and κ is the Thomson opacity (in units of $0.2 \text{ cm}^2 \text{ g}^{-1}$); κ may be significantly increased by pair creation. For the most powerful explosions ($L_\gamma \sim 10^{53} - 10^{54} \text{ erg s}^{-1}$) with relatively low Lorentz factors ($\Gamma \lesssim 10^2$) the photospheric radius is exceptionally large. If the GRB radiation is produced at a smaller radius R_{diss} (where internal dissipation peaks) the burst may be buried by the large optical depth, since it implies strong adiabatic cooling of the radiation trapped in the expanding ejecta.

To illustrate this possibility, suppose that the GRB emission is generated before the ejecta reaches a radius

$$R_{\text{diss}} = \Gamma^2 R_0, \quad (10)$$

where R_0 is a fixed constant. The scaling of the cutoff radius $R_{\text{diss}} \propto \Gamma^2$ is expected for mechanisms that dissipate the energy of internal motions or magnetic energy. Combining Equations (9) and (10), one finds the optical depth at R_{diss} ,

$$\tau_{\text{diss}} = \frac{R_*}{R_{\text{diss}}} \propto L \Gamma^{-5}. \quad (11)$$

If dissipation occurs far below the photosphere ($\tau_{\text{diss}} \gg 1$), the resulting radiation released at the photosphere is adiabatically cooled by the factor of $2\tau_{\text{diss}}^{-2/3}$ (Beloborodov 2011). Then for given

ejecta power L and dissipation efficiency at R_{diss} the observed burst luminosity scales as

$$L_\gamma \propto \Gamma^{10/3}. \quad (12)$$

The slope of this relation is suggestively close to the slope of $\Gamma_{\text{min}} - L_\gamma$ relation seen in Figure 2.

4.2. Properties of adiabatically cooled bursts

Even though the dissipation mechanism at $r < R_{\text{diss}}$ can be non-thermal, the produced radiation will be progressively thermalized during the subsequent adiabatic expansion between R_{diss} and R_* . Let T_e be the electron temperature (measured in the ejecta frame), and $\tau_{\text{diss}} > 1$ be the Thomson optical depth at R_{diss} . Two different regimes can be distinguished: (1) For $\tau_{\text{diss}} \lesssim m_e c^2 / 3kT_e \simeq 511 (3kT_e / 1 \text{ keV})^{-1}$, an exponential cutoff would form in the radiation spectrum at energy

$$E_{\text{max}} \approx \frac{\Gamma m_e c^2}{\tau_{\text{diss}}} \approx 511 \frac{\Gamma}{\tau_{\text{diss}}} \text{ keV}. \quad (13)$$

This cutoff is a result of significant Compton downscattering (recoil effect) at $E > E_{\text{max}}$; the spectrum at $E < E_{\text{max}}$ is weakly affected. (2) For $\tau_{\text{diss}} \gtrsim m_e c^2 / 3kT_e$, the spectrum is exponentially suppressed above $3kT_e \Gamma$. The low-energy part of the spectrum is also affected by multiple Compton scattering — the spectral slope steepens as the photons tend to thermalize with electrons.

Thus, one expects significant changes in the burst spectrum after strong adiabatic cooling. Such unusual GRBs have been observed. Ghirlanda et al. (2003) and Ryde (2004) found that some bursts have spectra with very hard low energy indices and possibly exponential cutoffs. Similar quasi-thermal GRBs are found in both BATSE (Kaneko et al. 2006) and Fermi Gamma Burst Monitor (Goldstein et al. 2012) catalogs. These bursts — especially those with a low peak energy — may be generated by adiabatically cooled explosions with a large photospheric radius R_* .

Another expected feature of bursts with small Γ and large R_* is the suppression of variability on short timescales. In these bursts, the minimum variability timescale $\Delta t_{\text{obs}} \sim R_*/2\Gamma^2 c$ can be as large as 10 s (see Equation (17) below), and their lightcurves are expected to be smooth.

While adiabatic cooling can significantly reduce the emitted GRB energy E_γ , the ejecta energy E_{ej} remains large. Thus, adiabatically cooled bursts are expected to have unproportionally bright afterglows. They should lie in the upper part of the gamma-ray fluence/X-ray afterglow flux distribution, which spreads over two orders of magnitude (see for example Fig. 2 in Gehrels et al. 2008). As we show below, the majority of GRBs with strong adiabatic cooling avoid detection. Then they become prime candidates for “orphan” afterglows (e.g. Huang et al. 2002). These afterglows are expected to peak at late times T_p , as they are generated by the low- Γ ejecta.

4.3. Monte Carlo simulation of a GRB population

To illustrate how bright bursts with low Lorentz factors are depleted by adiabatic cooling, we produced a synthetic GRB population using a Monte Carlo simulation, with the following assumptions:

- (1) We adopted the GRB rate R_{SF3} from Porciani & Madau (2001). We assume that the rate keeps increasing at $z \gtrsim 2$ as suggested by observations (e.g. Daigne et al. 2006; Wanderman & Piran 2010; Salvaterra et al. 2012); we cut it off at $z_{\max} \simeq 20$.
- (2) The GRB luminosity function is assumed to follow a power-law distribution of index -1.5 as suggested by Daigne et al. (2006), in a broad range of $10^{50} < L_\gamma < 10^{54}$ erg s $^{-1}$.
- (3) For each GRB, the spectrum of generated radiation at R_{diss} is assumed to be a broken power-law with a low energy index $\alpha = -1$ and a high energy index $\beta = -2.5$. The rest-frame peak energy of the spectrum, E_p , is assumed to correlate with L_γ ; we use the relation $E_p \simeq 300 (L_\gamma/10^{52} \text{ erg s}^{-1})^{1/2}$ keV with a scatter $\sigma_{\text{dex}} = 0.3$ (e.g. Wei & Gao 2003; Yonetoku et al. 2004; Nava et al. 2012).
- (4) The radiation spectrum is injected with $\eta = 0.5$ at $R_{\text{diss}} = 6 \times 10^{12} (\Gamma/100)^2$ cm (which would correspond to a variability timescale $\Delta t_{\text{obs}} = R_{\text{diss}}/2\Gamma^2 c \simeq 10$ ms if $R_{\text{diss}} > R_*$).
- (5) The logarithm of Lorentz factor Γ is randomly chosen for each burst from a uniform distribution in the range $1 < \log \Gamma < 3$.

The adiabatic cooling effect is calculated as follows:

- (6) The photospheric radius of each GRB is obtained from Equation (9), with $\kappa_{0.2} = 1$. If $R_{\text{diss}} < 2^{-3/2} R_*$, the burst is cooled by a factor of $2(R_*/R_{\text{diss}})^{-2/3}$ changing L_γ and E_p from their initial values at R_{diss} . The burst spectrum is changed as explained in Section 4.2; the cutoff at E_{max} is approximated by a step function.
- (7) The simulated GRB is assumed to be detected if its observed photon flux in the *Swift* band 15 – 150 keV is above the threshold of $0.2 \text{ ph cm}^{-2} \text{ s}^{-1}$ (Band 2006).

The results of our simulation are shown in Figure 5. One can see that adiabatic cooling depletes the low- Γ /high- L_γ corner of the $L_\gamma - \Gamma$ diagram. The resulting distribution resembles the observed one in Figure 2. This simulation also allows one to estimate the impact of adiabatic cooling on the observed distribution of E_p (Figure 6). A burst that suffers adiabatic cooling is moved along a track $E_p \propto L_\gamma$, which tends to create GRBs with E_p below the original correlation. However, the effect on the population of detected GRBs is weak, because cooled bursts become undetected (due to the reduced E_p and the spectral cutoff at E_{max}) before they become outliers in the $E_p - L_\gamma$ correlation.

5. Discussion

5.1. Adiabatic cooling

If the peak time of optical afterglow, T_p , is indeed a good proxy for the blast wave deceleration radius R_{dec} , observations imply a lack of bright bursts with low Lorentz factors (Section 3). We argued that this lack may be expected, as energetic explosions with low Lorentz factors should have unusually large photospheres $R_* \gtrsim 10^{15}$ cm. Since the dissipation mechanism generating radiation in these bursts is likely limited to smaller radii, $R_{\text{diss}} \ll R_*$, the burst is expected to suffer strong adiabatic cooling and become undetectable (Section 4).

Most models of the prompt GRB emission place the emission source at radii smaller than 10^{15} cm, especially if Γ is small. For example, dissipation of internal motions or magnetic energy in the ejecta is expected to end at a radius that scales as Γ^2 and becomes smaller than R_* at small Γ . Then the trapped radiation is adiabatically cooled and the burst becomes inefficient. This argument is applicable to any dissipation mechanism generating the burst — e.g. collisionless shocks (Rees & Meszaros 1994; Daigne & Mochkovitch 1998), collisional heating (Beloborodov 2010), or magnetic reconnection (Spruit et al. 2001). Note also that the neutron component of the jet, which can play a significant role in collisional dissipation, may not survive to R_* in low- Γ bursts. The mean radius of neutron decay is $R_\beta \simeq 9 \times 10^{13}(\Gamma/30)$ cm, and its ratio to the photospheric radius is given by

$$\frac{R_\beta}{R_*} \simeq 7.5 \times 10^{-2} \kappa_{0.2}^{-1} L_{54}^{-1} \left(\frac{\Gamma}{30}\right)^4 \ll 1. \quad (14)$$

The cooled bursts still produce energetic ejecta that can drive an energetic blast wave in the external medium and generate bright afterglow emission. We argued that one could observe “orphan” afterglows from such explosions, with undetected prompt GRBs, even when the burst is observed “on-axis,” i.e. the relativistic jet is directed toward the observer. As this paper was completed, Palomar Transient Factory detected an event consistent with on-axis orphan afterglow (Cenko et al. 2013).

We also argued that the prompt emission of strongly cooled bursts can be occasionally detected. As discussed in Section 4, these bursts have special properties. They should have soft spectra resembling quasi-thermal emission and their light curves should be smooth.

5.2. GRB ambient medium: a low density wind?

As some long GRBs are associated with Type Ib,c supernovae, their progenitors are expected to be Wolf-Rayet stars. Wolf-Rayet stars in our galaxy are observed to lose mass at a typical rate $\dot{M} \sim 10^{-5} M_\odot \text{ yr}^{-1}$ through strong winds of velocity $w \sim 10^8 \text{ cm s}^{-1}$ (e.g. Crowther 2007). If the

wind has constant \dot{M} , its density follows the R^{-2} density profile,

$$\rho(R) = \frac{A}{R^2}, \quad (15)$$

where

$$A = \frac{\dot{M}}{4\pi w} \simeq \left(\frac{\dot{M}}{10^{-5} M_\odot \text{ yr}^{-1}} \right) w_8^{-1} A_0, \quad A_0 = 5 \times 10^{11} \text{ g cm}^{-1}. \quad (16)$$

As discussed in Section 3, the peak time T_p of the optical afterglow provides an estimate of the ejecta Lorentz factor $\Gamma \approx \Gamma_{\text{bw}}$ if $T_p \gg T_\gamma$. This estimate scales as $\rho_{\text{dec}}^{-1/8}$. On the other hand, an independent constraint on Γ can be derived by considering the Thomson opacity of the ejecta and its photosphere.³ The photospheric radius R_* (Equation (9)) implies a minimum variability timescale $\Delta t_{\text{obs}} \approx R_*/2\Gamma^2 c$. Thus, the observed Δt_{obs} is expected to satisfy the condition,

$$\frac{\Delta t_{\text{obs}}}{1+z} \gtrsim \frac{R_*}{2\Gamma^2 c} \approx 5 \kappa_{0.2} \frac{1-\eta}{\eta} L_{\gamma,52} \Gamma_2^{-5} \text{ ms}. \quad (17)$$

From this condition, using the observed L_γ and Δt_{obs} , one obtains a lower bound on the ejecta Lorentz factor. Then, combining Equations (5) and (17), an upper limit on ρ_{dec} can be derived. For a wind medium this limit translates into an upper bound on A ,

$$A < A_{\text{max}} \approx 10^{11} \kappa_{0.2}^{-4/5} \left(\frac{1-\eta}{\eta} \right)^{1/5} E_{\gamma,52}^{1/5} \left(\frac{\Delta t_{\text{obs}}}{1+z} \right)^{4/5} T_\gamma^{4/5} T_{p,2}^{-1} \text{ g cm}^{-1}. \quad (18)$$

This upper limit is sensitive to the Thomson opacity κ , which may be significantly increased by e^\pm creation in the ejecta. The numerical value for A_{max} in Equation (18) is given for the lowest possible $\kappa = 0.2 \text{ cm}^2 \text{ g}^{-1}$, which gives a conservative upper limit on A . Figure 7 shows the upper limits obtained for our GRB sample, where we used $\eta = 0.5$, $\kappa_{0.2} = 1$, and $\Delta t_{\text{obs}} = 1 \text{ s}$. In some bursts, the inferred A_{max} is well below A_0 . For GRB 060605, A_{max} is ~ 6 times smaller than A_0 . Even stronger limits could be derived with more sensitive detectors and more detailed analysis of variability timescales. GRBs that give the lowest A_{max} have relatively low luminosities, and poor photon statistics make it difficult to see the true minimum Δt_{obs} , which might be shorter than 1 s.

Figure 7 suggests that at least some GRB progenitors are peculiar massive stars whose winds are weaker than typical Wolf-Rayet stars observed in our galaxy. This may be the result of a lower metallicity of the star (e.g. Vink et al. 2001), a property that seems to be preferred by GRB progenitors, and agrees with observations of their host galaxies (e.g. Perley et al. 2013). Weaker winds extract less angular momentum from the progenitor, leading to collapse with faster rotation, which is required for GRB central engines producing collimated jets (e.g. Woosley & Heger 2006). Note also that GRBs with bright optical afterglows (such as bursts in our sample) imply a selection

³For GRBs with detected high-energy emission (above 100 MeV) another constraint on Γ could be derived from the requirement that the high-energy photons avoid γ - γ absorption (e.g. Lithwick & Sari 2001; Granot et al. 2008; Hascoët et al. 2012). There are no such bursts in our sample.

against high-metallicity environment, which tends to obscure the optical emission (e.g. Levesque 2013).

The low wind density could also be explained by a change in the stellar mass loss rate \dot{M} shortly before the explosion. The wind medium at a characteristic radius $R_{\text{dec}} \sim 10^{16}$ cm was ejected by the progenitor $R_{\text{dec}}/w \sim 3$ yr before the explosion. The mass loss rates of Wolf-Rayet stars in the last few years of their lives are uncertain; \dot{M} might decrease as the star evolves toward the collapse.

This work was supported by NSF grant AST-1008334.

REFERENCES

- Band, D. L. 2006, *ApJ*, 644, 378
- Beloborodov, A. M. 2002, *ApJ*, 565, 808
- . 2010, *MNRAS*, 407, 1033
- . 2011, *ApJ*, 737, 68
- Berger, E., Fox, D. B., Cucchiara, A., & Cenko, S. B. 2008, *GRB Coordinates Network*, 8335, 1
- Bloom, J. S., Foley, R. J., Kocevski, D., & Perley, D. 2006, *GRB Coordinates Network*, 5217, 1
- Blustin, A. J., Band, D., Barthelmy, S., et al. 2006, *ApJ*, 637, 901
- Butler, N. R., Li, W., Perley, D., et al. 2006, *ApJ*, 652, 1390
- Cenko, S. B., Kulkarni, S. R., Horesh, A., et al. 2013, *ApJ*, 769, 130
- Chevalier, R. A., & Li, Z.-Y. 2000, *ApJ*, 536, 195
- Covino, S., Campana, S., Conciatore, M. L., et al. 2010, *A&A*, 521, A53
- Crew, G., Ricker, G., Atteia, J.-L., et al. 2005, *GRB Coordinates Network*, 4021, 1
- Crew, G. B., Lamb, D. Q., Ricker, G. R., et al. 2003, *ApJ*, 599, 387
- Crowther, P. A. 2007, *ARA&A*, 45, 177
- Cucchiara, A., & Fox, D. B. 2008, *GRB Coordinates Network*, 7654, 1
- Cummings, J., Barthelmy, S., Barbier, L., et al. 2006, *GRB Coordinates Network*, 5124, 1
- Cusumano, G., Mangano, V., Angelini, L., et al. 2006, *ApJ*, 639, 316

- Daigne, F., & Mochkovitch, R. 1998, MNRAS, 296, 275
- Daigne, F., Rossi, E. M., & Mochkovitch, R. 2006, MNRAS, 372, 1034
- de Pasquale, M., & Cummings, J. 2006, GRB Coordinates Network, 5130, 1
- Deng, J., Zheng, W., Zhai, M., et al. 2009, arXiv:0912.5435
- Filgas, R., Krühler, T., Greiner, J., et al. 2011, A&A, 526, A113
- Fugazza, D., Fiore, F., Patat, N., et al. 2005, GRB Coordinates Network, 3948, 1
- Fynbo, J. P. U., Jensen, B. L., Hjorth, J., et al. 2005, GRB Coordinates Network, 3176, 1
- Gehrels, N., Barthelmy, S. D., Burrows, D. N., et al. 2008, ApJ, 689, 1161
- Gendre, B., Klotz, A., Palazzi, E., et al. 2010, MNRAS, 405, 2372
- Genet, F., Daigne, F., & Mochkovitch, R. 2007, MNRAS, 381, 732
- Ghirlanda, G., Celotti, A., & Ghisellini, G. 2003, A&A, 406, 879
- Ghirlanda, G., Nava, L., Ghisellini, G., et al. 2012, MNRAS, 420, 483
- Goldstein, A., Burgess, J. M., Preece, R. D., et al. 2012, ApJS, 199, 19
- Golenetskii, S., Aptekar, R., Mazets, E., et al. 2005, GRB Coordinates Network, 4238, 1
- Goodman, J. 1986, ApJ, 308, L47
- Granot, J., Cohen-Tanugi, J., & do Couto e Silva, E. 2008, ApJ, 677, 92
- Grupe, D., Marshall, F. E., Cummings, J. R., et al. 2009, GCN Report, 260, 1
- Guidorzi, C., Stamatikos, M., Landsman, W., et al. 2008, GCN Report, 139, 1
- Guidorzi, C., Kobayashi, S., Perley, D. A., et al. 2011, MNRAS, 417, 2124
- Hascoët, R., Daigne, F., Mochkovitch, R., & Vennin, V. 2012, MNRAS, 421, 525
- Huang, K. Y., Urata, Y., Tung, Y. H., et al. 2012, ApJ, 748, 44
- Huang, Y. F., Dai, Z. G., & Lu, T. 2002, MNRAS, 332, 735
- Hunsberger, S. D., Marshall, F., Holland, S. T., et al. 2005, GCN Report, 4041, 1
- Jelinek, M., Kubanek, P., Gorosabel, J., et al. 2008, GRB Coordinates Network, 7648, 1
- Kaneko, Y., Preece, R. D., Briggs, M. S., et al. 2006, ApJS, 166, 298
- Krimm, H., Barbier, L., Barthelmy, S., et al. 2005a, GRB Coordinates Network, 4020, 1

- Krimm, H., Ajello, M., Barbier, L., et al. 2005b, GRB Coordinates Network, 4260, 1
- Landsman, W. B., & Guidorzi, C. 2008, GRB Coordinates Network, 7660, 1
- Levesque, E. M. 2013, arXiv:1302.4741
- Li, W., Filippenko, A. V., Chornock, R., & Jha, S. 2003, ApJ, 586, L9
- Liang, E.-W., Yi, S.-X., Zhang, J., et al. 2010, ApJ, 725, 2209
- Liang, E.-W., Li, L., Gao, H., et al. 2013, ApJ, 774, 13
- Lithwick, Y., & Sari, R. 2001, ApJ, 555, 540
- Lü, J., Zou, Y.-C., Lei, W.-H., et al. 2012, ApJ, 751, 49
- Markwardt, C. M., Barthelmy, S. D., Baumgartner, W. H., et al. 2008, GRB Coordinates Network, 8338, 1
- Martin-Carrillo, A., Hanlon, L., McGlynn, S., et al. 2008, in Proc. 7th INTEGRAL Workshop, 2008 September 8–11 (Proceedings of Science: Copenhagen, Denmark), 16
- Meszáros, P., & Rees, M. J. 1997, ApJ, 476, 232
- Molinari, E., Vergani, S. D., Malesani, D., et al. 2007, A&A, 469, L13
- Nava, L., Salvaterra, R., Ghirlanda, G., et al. 2012, MNRAS, 421, 1256
- Oksanen, A., & Hentunen, V.-P. 2008, GRB Coordinates Network, 7657, 1
- Paczynski, B. 1986, ApJ, 308, L43
- Page, K. L., Starling, R. L. C., Fitzpatrick, G., et al. 2011, MNRAS, 416, 2078
- Pandey, S. B., Anupama, G. C., Sagar, R., et al. 2003, A&A, 408, L21
- Perley, D. A., Li, W., Chornock, R., et al. 2008, ApJ, 688, 470
- Perley, D. A., Levan, A. J., Tanvir, N. R., et al. 2013, arXiv:1301.5903
- Piran, T. 2004, Reviews of Modern Physics, 76, 1143
- Porciani, C., & Madau, P. 2001, ApJ, 548, 522
- Quimby, R. M., Rykoff, E. S., Yost, S. A., et al. 2006, ApJ, 640, 402
- Racusin, J. L., Karpov, S. V., Sokolowski, M., et al. 2008, Nature, 455, 183
- Rees, M. J., & Meszaros, P. 1994, ApJ, 430, L93

- Ryde, F. 2004, *ApJ*, 614, 827
- Rykoff, E. S., Yost, S. A., Krimm, H. A., et al. 2005, *ApJ*, 631, L121
- Rykoff, E. S., Aharonian, F., Akerlof, C. W., et al. 2009, *ApJ*, 702, 489
- Sakamoto, T., Barthelmy, S., Barbier, L., et al. 2005, *GRB Coordinates Network*, 3173, 1
- Salvaterra, R., Campana, S., Vergani, S. D., et al. 2012, *ApJ*, 749, 68
- Sari, R., & Piran, T. 1999, *A&AS*, 138, 537
- Sari, R., Piran, T., & Narayan, R. 1998, *ApJ*, 497, L17
- Sato, G., Barbier, L., Barthelmy, S., et al. 2005, *GRB Coordinates Network*, 3951, 1
- Sollerman, J., Fynbo, J. P. U., Gorosabel, J., et al. 2007, *A&A*, 466, 839
- Spruit, H. C., Daigne, F., & Drenkhahn, G. 2001, *A&A*, 369, 694
- Stamatikos, M., Barthelmy, S. D., Cummings, J., et al. 2007, *GRB Coordinates Network*, 7029, 1
- Stamatikos, M., Cummings, J. R., Evans, P. A., et al. 2009, *GRB Coordinates Network*, 9768, 1
- Starling, R. L. C., Rol, E., van der Horst, A. J., et al. 2009, *MNRAS*, 400, 90
- Thompson, C., & Madau, P. 2000, *ApJ*, 538, 105
- Uehara, T., Toma, K., Kawabata, K. S., et al. 2012, *ApJ*, 752, L6
- Uhm, Z. L., & Beloborodov, A. M. 2007, *ApJ*, 665, L93
- Ukwatta, T. N., Barthelmy, S. D., Baumgartner, W. H., et al. 2008, *GRB Coordinates Network*, 8599, 1
- Vink, J. S., de Koter, A., & Lamers, H. J. G. L. M. 2001, *A&A*, 369, 574
- Wanderman, D., & Piran, T. 2010, *MNRAS*, 406, 1944
- Wei, D. M., & Gao, W. H. 2003, *MNRAS*, 345, 743
- Wiersema, K., van der Horst, A. J., Kann, D. A., et al. 2008, *A&A*, 481, 319
- Wiersema, K., Curran, P. A., Krühler, T., et al. 2012, *MNRAS*, 426, 2
- Woosley, S. E., & Heger, A. 2006, *ApJ*, 637, 914
- Wren, J., Vestrand, W. T., Wozniak, P. R., Davis, H., & Norman, B. 2008, *GRB Coordinates Network*, 8337, 1

Yonetoku, D., Murakami, T., Nakamura, T., et al. 2004, ApJ, 609, 935

Yuan, F., Schady, P., Racusin, J. L., et al. 2010, ApJ, 711, 870

Zaninoni, E., Bernardini, M. G., Margutti, R., Oates, S., & Chincarini, G. 2013, A&A, 557, A12

Table 2: Bursts with upper limits on T_p .

| GRB | z | $E_{\gamma,52}$ | T_p^{obs} | T_{90} | References |
|---------|---------|------------------|--------------------|-----------------|--------------------|
| 021211 | 1.004 | 1.02 ± 0.1 | < 130 | 3.5 ± 0.5 | 1, 2, 3 |
| 040924 | 0.858 | 1.5 ± 0.5 | < 870 | 2.39 ± 0.24 | 4 |
| 050319 | 3.24 | 3.7 ± 1 | < 164 | 149.6 ± 0.7 | 5, 6 |
| 050401 | 2.9 | 26 ± 1 | < 36 | 33 ± 2 | 7, 8, 9 |
| 050525A | 0.606 | 2.3 ± 1 | < 70 | 8.8 ± 0.5 | 10 |
| 050824 | 0.828 | 0.19 ± 0.05 | < 700 | 25 ± 1 | 11 |
| 050908 | 3.35 | 1.36 ± 0.1 | < 300 | 20 ± 2 | 12, 13, 14 |
| 050922C | 2.17 | 3.7 ± 1 | < 116 | 5 ± 1 | 15, 16, 17 |
| 051109A | 2.346 | 3 ± 1 | < 35 | 37 ± 5 | 18, 19 |
| 051111 | 1.55 | 7 ± 1 | < 27 | 47 ± 1 | 20, 21 |
| 060512A | 0.4428 | 0.02 ± 0.005 | < 94 | 8.6 ± 2 | 22, 23, 24 |
| 060908 | 1.884 | 6.2 ± 0.7 | < 61 | 19.3 ± 0.3 | 25 |
| 060912 | 0.937 | 0.85 ± 0.15 | < 99 | 7 ± 1 | 26 |
| 071003 | 1.60435 | 34 ± 4 | < 42 | 148 ± 1 | 27 |
| 071112C | 0.823 | 0.53 ± 0.1 | < 100 | 15 ± 12 | 28 |
| 080319B | 0.937 | 130 ± 10 | < 70 | 55 ± 5 | 29 |
| 080413B | 1.1 | 1.8 ± 0.5 | < 77 | 8.0 ± 1 | 30 |
| 080430 | 0.767 | 0.3 ± 0.1 | < 60 | 16.2 ± 2.4 | 31, 32, 33, 34, 35 |
| 080721 | 2.591 | 130 ± 10 | < 164 | 16.2 ± 4.5 | 36 |
| 081007 | 0.5295 | 0.1 ± 0.02 | < 140 | 10.0 ± 4.5 | 37, 38, 39 |
| 090102 | 1.547 | 57.5 ± 5 | < 44 | 27 ± 2.2 | 40 |
| 090618 | 0.54 | $25. \pm 1$ | < 100 | 113 ± 1 | 41 |
| 091018 | 0.971 | 0.37 ± 0.1 | < 147 | 4.4 ± 0.6 | 42 |
| 091208B | 1.063 | 1 ± 0.2 | < 80 | 14.9 ± 3.7 | 43 |

References: (1) Crew et al. 2003; (2) Li et al. 2003; (3) Pandey et al. 2003; (4) Wiersema et al. 2008; (5) Cusumano et al. 2006; (6) Quimby et al. 2006; (7) Sakamoto et al. 2005; (8) Fynbo et al. 2005; (9) Rykoff et al. 2005; (10) Blustin et al. 2006; (11) Sollerman et al. 2007; (12) Sato et al. 2005; (13) Fugazza et al. 2005; (14) Zaninoni et al. 2013; (15) Hunsberger et al. 2005; (16) Crew et al. 2005; (17) Krimm et al. 2005a; (18) Rykoff et al. 2009; (19) Golenetskii et al. 2005; (20) Butler et al. 2006; (21) Krimm et al. 2005b; (22) Cummings et al. 2006; (23) Bloom et al. 2006; (24) de Pasquale & Cummings 2006; (25) Covino et al. 2010; (26) Deng et al. 2009; (27) Perley et al. 2008; (28) Huang et al. 2012; (29) Racusin et al. 2008; (30) Filgas et al. 2011; (31) Jelinek et al. 2008; (32) Landsman & Guidorzi 2008; (33) Oksanen & Hentunen 2008; (34) Cucchiara & Fox 2008; (35) Guidorzi et al. 2008; (36) Starling et al. 2009; (37) Markwardt et al. 2008; (38) Wren et al. 2008; (39) Berger et al. 2008; (40) Gendre et al. 2010; (41) Page et al. 2011; (42) Wiersema et al. 2012; (43) Uehara et al. 2012

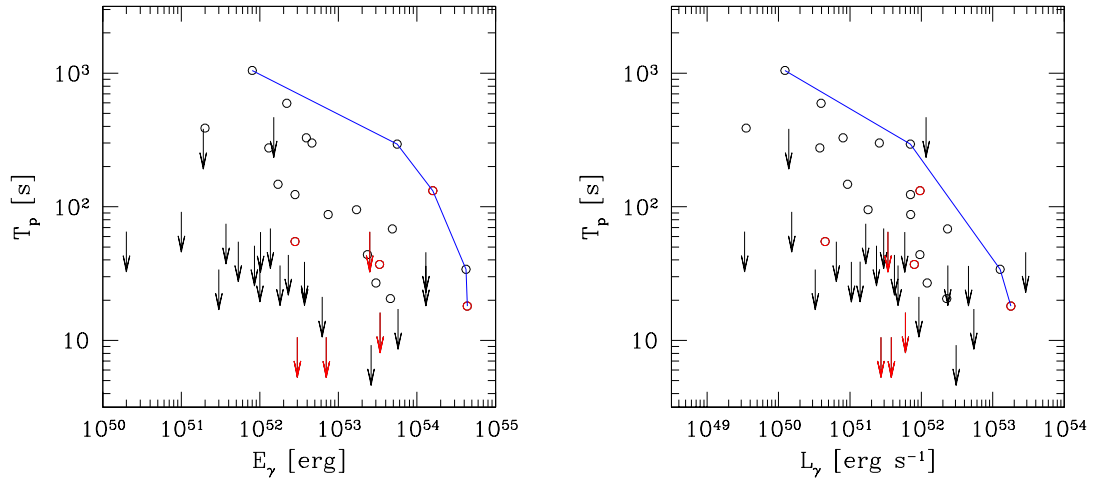


Fig. 1.— Bursts on $T_p - E_\gamma$ and $T_p - L_\gamma$ planes. Circles represent bursts with detected T_p , and arrows show upper limits. Bursts with $T_p < T_\gamma$ are shown by red circles and arrows. The blue line shows the observed boundary of the burst population.

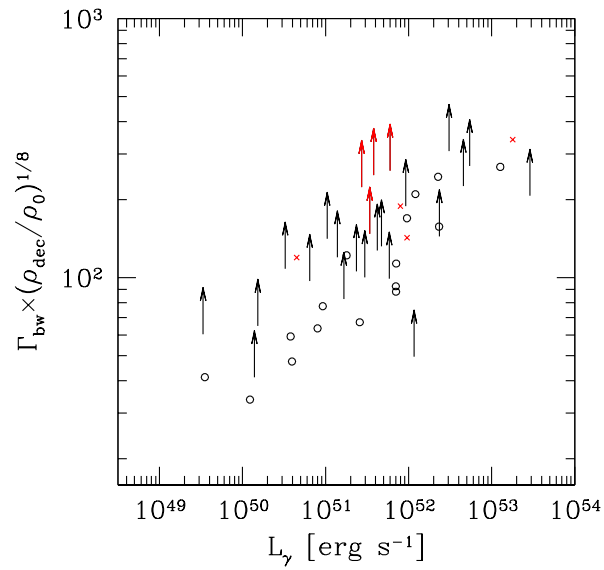


Fig. 2.— Estimated Lorentz factor of the GRB blast wave, Γ_{bw} , at the deceleration radius. The product $\Gamma_{\text{bw}} \rho_{\text{dec}}^{1/8}$ is estimated using Equation (5) (with $\eta = 0.5$) and shown versus the burst luminosity L_γ (Equation (2)). The ambient density at the deceleration radius, ρ_{dec} , is normalized to $\rho_0/m_p = 1 \text{ cm}^{-3}$. Bursts with $T_p < T_\gamma$ are highlighted in red; for these bursts the ejecta Lorentz factor Γ can be substantially higher than Γ_{bw} (see text).

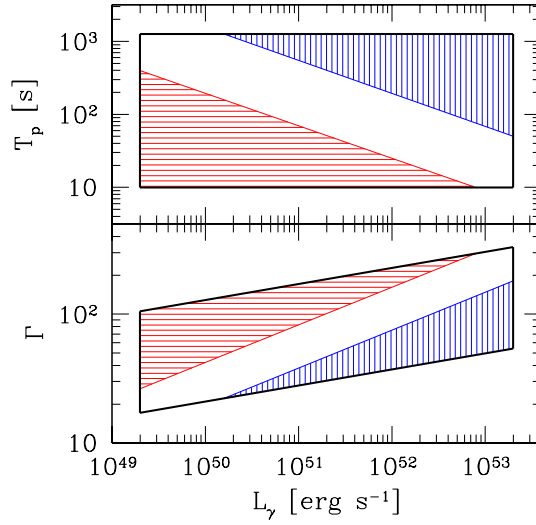


Fig. 3.— Effects of the $T_p \rightarrow \Gamma$ transformation. This schematic figure illustrates how the GRB population presented in Figure 1 ($T_p - L_\gamma$ plane) transforms into the $\Gamma - L_\gamma$ plane. The hatched and colored areas are indicated to better visualize how different regions on the $T_p - L_\gamma$ plane transform to the $\Gamma - L_\gamma$ plane. The red (horizontally hatched) region is where strong selection effects are expected to suppress the observed population. Combined with the real lack of bursts in the blue (vertically hatched) region, this leads to a spurious correlation between T_p and L_γ . The corresponding spurious $\Gamma - L_\gamma$ correlation is enhanced by the deformation of the population in the $\Gamma - L_\gamma$ coordinates – the black rectangular in the upper panel is transformed into a “parallelogram” in the lower panel.

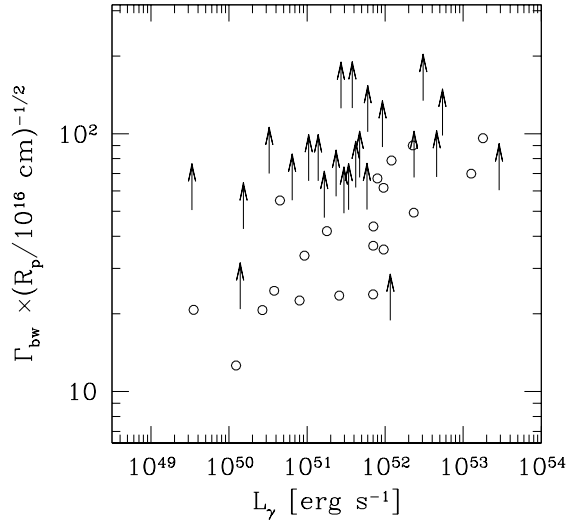


Fig. 4.— Estimated Lorentz factor of the GRB blast wave $\Gamma_{\text{bw}} = (R_p/2cT_p)^{1/2}$ for an arbitrarily fixed afterglow peak radius R_p . The product $\Gamma_{\text{bw}}R_p^{-1/2}$ shown in this figure is proportional to $T_p^{-1/2}$, so the diagram is a simple transformation of the $T_p - L_\gamma$ diagram shown in Figure 1.

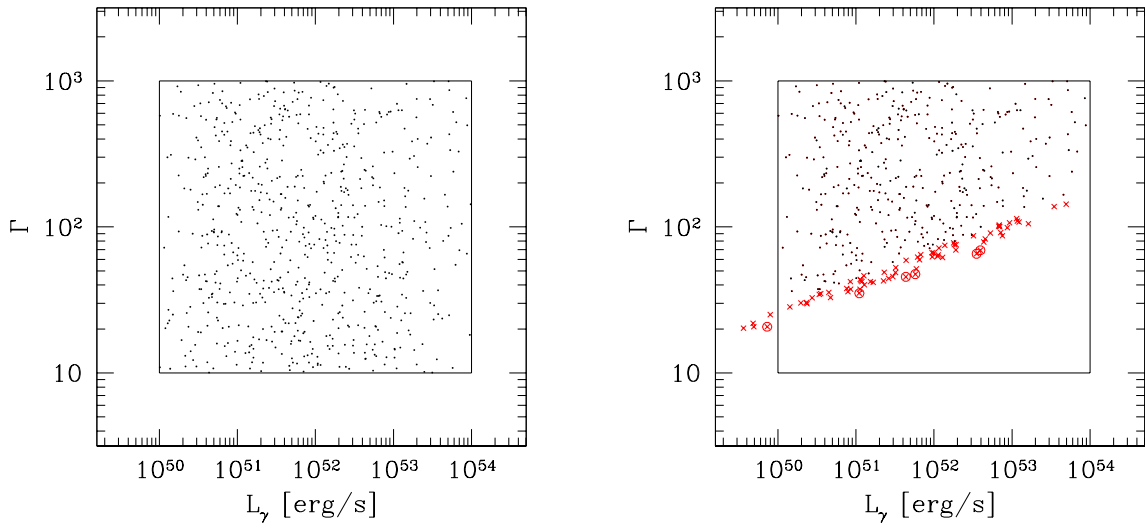


Fig. 5.— Effect of adiabatic cooling on a GRB population in the $L_\gamma - \Gamma$ plane. *Left:* observed distribution of bursts when adiabatic cooling is not included. *Right:* observed distribution of bursts when adiabatic cooling is included. Red crosses represent bursts that have suffered cooling and remained detectable. Many more cooled bursts became undetectable and disappeared from the diagram. The circled red crosses show detected bursts with large cooling factors $f > 10$ (1.3% of detected bursts). These bursts are expected to have special spectra of the prompt GRB emission (see text).

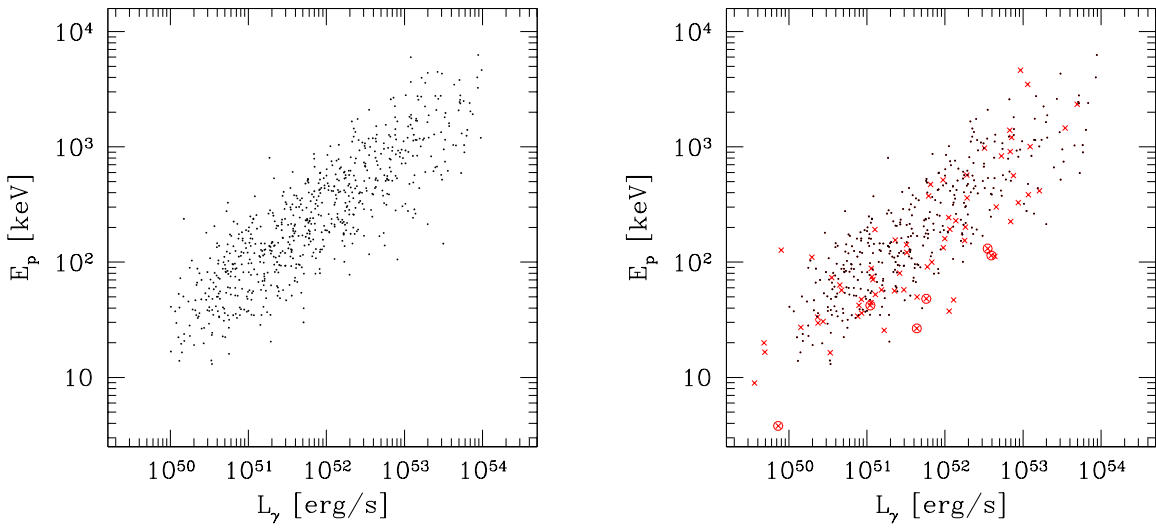


Fig. 6.— Effect of adiabatic cooling on a GRB population in the $L_\gamma - E_p$ plane. The simulation is the same as in Figure 5. *Left:* observed distribution of bursts when adiabatic cooling is not included. *Right:* observed distribution of bursts when adiabatic cooling is included. Red crosses represent bursts that have suffered cooling. The circled red crosses show detected bursts with large cooling factors $f > 10$ (1.3% of detected bursts). Strong adiabatic cooling can in principle create outliers of the initial $E_p - L_\gamma$ correlation, however most of them become undetectable and disappear from the diagram.

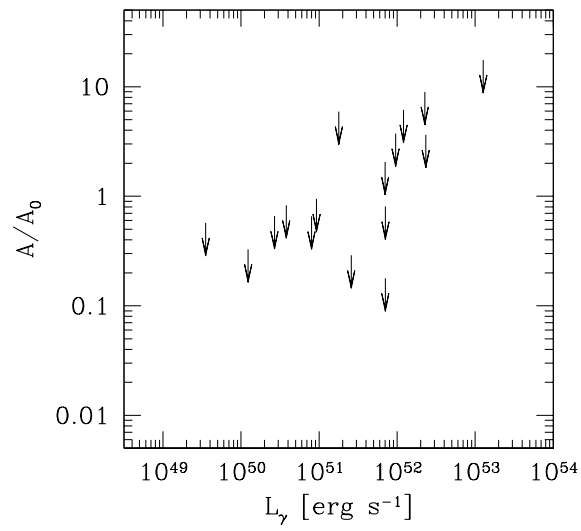


Fig. 7.— Constraints on the wind from the GRB progenitor. The figure shows the derived upper limits on the wind density parameter $A = \dot{M}/4\pi w$ in units of $A_0 = 5 \times 10^{11}$ g cm⁻¹.